10.1098/rsta.2004.1399

THE ROYAL SOCIETY

Molecular-dynamics simulation of amphiphilic bilayer membranes and wormlike micelles: a multi-scale modelling approach to the design of viscoelastic surfactant solutions

By E. S. Boek[1], W. K. den Otter[2], W. J. Briels[2] and D. Iakovlev[1,3]

[1]*Schlumberger Cambridge Research, High Cross, Madingley Road, Cambridge CB3 0EL, UK* (boek@cambridge.oilfield.slb.com)
[2]*Computational Dispersion Rheology, University of Twente, PO Box 217, 7500 Enschede, The Netherlands*
[3]*Department of Chemistry, St Petersburg State University, 26 Universitetsky pr., St Petersburg 198504, Russia*

Published online 2 June 2004

Bilayer membranes and wormlike micelles have been studied using molecular-dynamics simulations. The structure of the worm is analysed in terms of radial density distribution functions, and mechanical properties such as the elastic modulus are calculated. From an analysis of the fluctuation spectra of the tensionless states, we have calculated bending rigidities. Micelles consisting of coarse-grained (CG) model surfactants are studied in order to map the properties of the atomistic micelle. We optimize the CG model with respect to the structure factor $S(\boldsymbol{q})$ of the atomistic micelle. The mechanical properties thus obtained will be used as input for a mesoscopic model of wormlike micelles where the persistence length is the smallest length-scale.

Keywords: membrane; wormlike micelle; bending rigidity; viscoelastic surfactant; MD simulation

1. Introduction

In hydrocarbon recovery processes there is an increasing need for responsive fluids which can transform their characteristics from low-viscosity, Newtonian behaviour to a highly viscoelastic gel then back to a low-viscosity liquid. This is required at different stages of a reservoir treatment process in response to chemical or physical triggers that either occur naturally in the process or can be imposed externally. Surfactant self-assembly and disassembly is one route for achieving this, and viscoelastic surfactants operating in the wormlike micelle regime are being increasingly used as reservoir stimulation fluids. This paper describes the use of molecular-dynamics (MD) simulations to improve understanding of the structure and mechanical properties of the surfactant phase.

One contribution of 21 to a Theme 'Connecting scales: micro, meso and macro processes'.

© 2004 The Royal Society

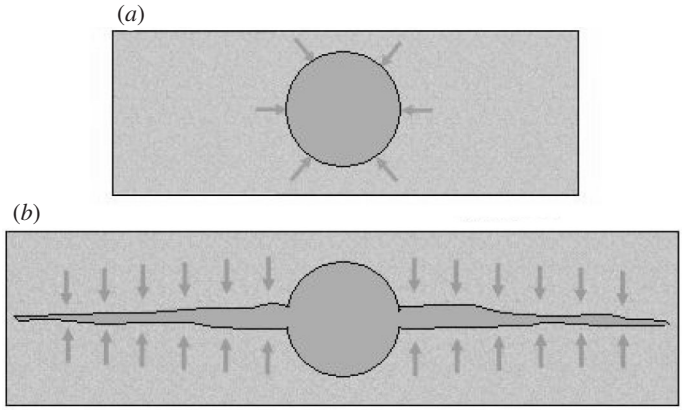

Figure 1. Schematic of an oil well in cross-section illustrating (*a*) how oil production can be limited due to radial flow into the well. The hydraulic creation of two opposing vertical fractures (*b*) extending up to 300 m from the well gives large productivity increases due to linear flow into the highly conductive fracture. This is propped open by sand transported into the fracture during its creation by the viscoelastic fracturing fluid, preventing closure when the pressure is reduced and production begins. The permeability of this packed bed is crucial to the enhancement of oil production.

The nature of the oilfield applications and of the viscoelastic surfactant (VES) fluids will first be described. Then, given that MD simulations can only simulate such complex fluids for a few nanoseconds at most, we describe our approach for bridging the time- and length-scales required to predict their bulk behaviour. The main focus of this paper is to investigate the effect of changes in head group structure on the mechanical properties of the micelles. Note that we use pre-assembled membranes for computational reasons (Ben-Shaul & Gelbart 1994). First, our model used to simulate the lamellar phase will be described and MD results presented, showing how the mechanical properties of the surfactant membrane change significantly with relatively small modifications to head group structure. The results are compared with MD simulations for bilayer membranes of coarse-grained (CG) surfactants. Finally, some results of recent work on MD simulations of wormlike micelles will be presented.

2. Oilfield applications and fluid requirements for VES fluids

Once an oil well has been constructed, its production can be limited by low natural reservoir permeability or by permeability reductions induced by particulate damage to the rock pore space during either drilling or production. The creation of hydraulic fractures is one major stimulation process commonly used to overcome these limitations.

The most common fracturing fluids use natural polymers, such as guar, sometimes cross-linked to form viscoelastic gels. These fluids transmit hydraulic pressure to the rock to induce fractures in the formation, into which sand or other ceramic particles ('proppant') are transported by the gel, to give a porous proppant pack which keeps the fractures open on removal of the fluid pressure (see figure 1). Once the proppant is in place, delayed oxidative or enzymatic breakers are used to degrade the gel retained within the proppant pack.

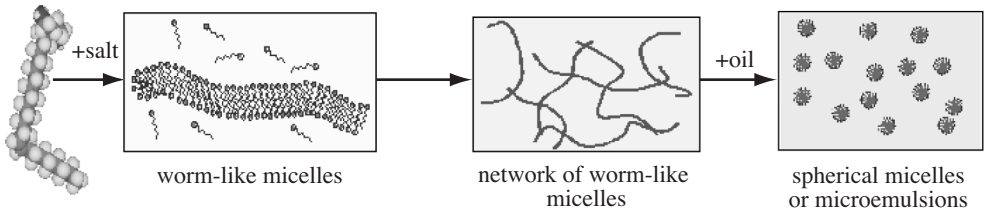

Figure 2. Schematic of the production of wormlike micelles and their destruction by oil.

A serious limitation of many of these polymeric fluids is that, despite the gel-breaking step, small cross-linked fragments, comparable in size to the sandpack pore throats, reduce the hydraulic conductivity of the pack significantly. A new generation of fracturing fluids based upon viscoelastic surfactants has recently been introduced, which attempts to address this problem. Their gel rheology is caused by wormlike cylindrical micelles (see figure 2). Once these come into contact with hydrocarbon produced from the fracture through the proppant pack, they revert to small spherical micelles or microemulsions, the fluid viscoelasticity falls by orders of magnitude, the fluid residues flow easily out of the pack and fracture flowback efficiencies of close to 100% are achieved.

Recent studies of microstructure and rheology for model wormlike micellar systems, such as cetyl trimethyl ammonium bromide (CTAB), provide the underpinning understanding of molecular-bulk property relationships to guide fluid design. Of particular significance for controlling applications is the strong coupling between shear flow and structure/phase behaviour for these systems. The general rheological behaviour of viscoelastic surfactants comprising wormlike micelles can be rationalized within the now classical framework of Cates (1988).

The principle of VES fracturing fluids is shown in figure 2. The surfactant, typically a C_{22} erucyl derivative, is activated by salt, which screens the head group charge interactions, to form wormlike micelles. These form a highly entangled network, giving rise to a high viscosity, shear-thinning and elastic solution at relatively low surfactant concentrations. Exposure to oil, typically *ca.* 1 wt %, causes the micelles to revert to spherical microemulsions with viscosities close to water. Raghavan & Kaler (2001) recently published a comprehensive study of the rheological behaviour of erucyl bis (2-hydroxyethyl) methyl ammonium chloride (EHAC), which demonstrates the characteristics typical of this type of fluid. The wormlike micelle regime can be activated by both non-binding and binding salts (e.g. sodium chloride and salicylate, respectively), where fluid viscosity goes through a maximum with salt concentration.

For oilfield applications, the ability to sustain high temperatures is particularly important. One design criterion is that the viscosity at a shear rate of $100\,s^{-1}$ must be greater than 50 mPa s. Changes in head group chemistry can markedly affect the temperature at which this fails to be achieved. EHAC is limited to temperatures below 85 °C, whereas replacing the hydroxyethyl groups by methyl reduces this temperature to *ca.* 70 °C (Raghavan & Kaler 2001). In contrast, replacing the quaternary cationic head group by the smaller anionic carboxylate group increases this critical temperature to over 100 °C.

It is our objective to gain a fundamental understanding of the relationship between microscopic interactions at the molecular level, and the macroscopic transport properties, and in particular the rheology, of viscoelastic surfactants, both in the bulk

fluid and in porous media. Starting from an atomistic-model description of the surfactant molecules, this will lead to a prediction of the rheology of wormlike micellar fluids from first principles. This will, in turn, lead to a method of designing and optimizing surfactant molecular structure for enhanced performance. Because MD simulations for the size of system needed to give a realistic model (at least 100 surfactant chains and orders of magnitude more water molecules) cannot reach macroscopic time-scales, a series of coarse graining steps is required to bridge the gap between MD simulation and bulk behaviour. This series of steps will be explained below.

The objective of a previous study (Boek *et al*. 2002) was to understand why these relatively small changes in head group structure cause such major changes in high-temperature rheology and, by inference, the stability of the wormlike phase. Using MD simulations, it was found that a bilayer membrane with carboxylate head groups develops a crystalline structure, where the erucyl tails are strongly ordered. The EHAC membrane, on the other hand, displays liquid-crystalline phase behaviour. Assuming that the local behaviour of the micellar surfactants is comparable for membranes and wormlike micelles, a qualitative correlation could be established with the experimental observation that the wormlike phase is stable up to higher temperatures for erucate than for EHAC surfactants.

In the present study, we use MD simulations to calculate the mechanical properties, such as the bending rigidity, of amphiphilic bilayer membranes and wormlike micelles. These mechanical properties serve as input parameters for the next level, where the wormlike micelles will be described using a mesoscopic model. This model is described in the following section.

3. Bridging the molecular and bulk length- and time-scales

Four levels of description are required to connect the microscopic and macroscopic length- and time-scales.

Atomistic MD: at this level, mechanical properties of atomistic micelles are calculated, such as persistence length l_{p}, elastic modulus K_L and scission energy E_{sc}.

Coarse-grained MD: micelles consisting of coarse-grained (CG) model surfactants are studied in order to map the properties of the atomistic micelle. Here, we optimize the CG model with respect to the structure factor $S(\boldsymbol{q})$ of the atomistic micelle at large values of the wavevector $\boldsymbol{q}$. The CG model is used to extrapolate the structure factor for small $\boldsymbol{q}$ in order to obtain reliable values for the micelle bending rigidity κ and persistence length l_{p}.

Mesoscale: at this level, we consider a mesoscopic model of wormlike micelles, represented by chains which can break and recombine and can be subjected to shear flow. For this model, where the smallest length-scale is the persistence length, we need the elastic modulus K_L, scission energy E_{sc} and persistence length l_{p} as input from the atomistic and CG MD. As output we expect to obtain the rheology of the wormlike micellar fluid from first principles.

Fluid dynamics: having obtained an accurate description of the bulk fluid rheology from the mesoscopic model described above, we can use this as an input to study

flow in constricted geometries such as flow in porous media or particle laden flows, using lattice Boltzmann (Boek *et al*. 2003) and related techniques.

4. Surfactants studied

In our studies, two types of surfactants were investigated, which differ only in their hydrophilic head group chemistry. They have the same hydrophobic part $CH_3(CH_2)_7CH{=}CH(CH_2)_{12}{-}$, which is a linear hydrocarbon chain $C_{22}H_{43}$ with a *cis*-double bond between the 9th and 10th carbon atoms (the atoms are counted from the CH_3 group). These surfactants have ionic head groups of the following types.

Erucate: an anionic surfactant with a negatively charged carboxylate head group ($-COO^-$) and sodium counterion;

EHAC: an cationic surfactant with a positively charged $-N^+(CH_2CH_2OH)_2CH_3$ (bis-(hydroxyethyl) methylammonium) head group and chloride counterion.

In some cases, sodium salicylate $C_6H_4(OH)COONa$ was added as solubilized admixture, which is found to be an effective viscosifier under experimental conditions.

5. MD simulation of surfactant bilayer membranes

The simulations were done using the Gromacs (Lindahl *et al*. 2001; Berendsen *et al*. 1995) and Dl_Poly (Smith & Forester 1996) program packages running in parallel under the MPI environment. Two different MD codes were used to compare the results for different force fields for bonded and non-bonded van der Waals interactions. Atomic net charges were the same for Gromacs and Dl_Poly simulations and were taken from semi-empirical calculations using the MNDO Hamiltonian model (see Boek *et al*. 2002). An orthogonal simulation box was used together with periodic boundary conditions in all dimensions. The bilayer formed by surfactant molecules was positioned in the middle of the box parallel to the (x, y)-plane. The rest of the box was filled with SPC water molecules (Berendsen *et al*. 1981) and counter ions. The bilayer membranes constructed contain either $11 \times 11 \times 2$ (EHAC) or $16 \times 8 \times 2$ (erucate) surfactant molecules. The number of water molecules was up to several thousand.

The simulations were carried out at a constant temperature of 300 K and a constant pressure of 1 bar using the leapfrog integration method with a time-step of 2 fs. The simulation cell was scaled isotropically in the x- and y-directions but independently in the z-direction (so-called 'semi-isotropic' coupling). The bonds were constrained by the Shake algorithm and its implementation for rigid three-atomic molecules Settle (Miyamoto & Kollman 1992). All interactions were subject to a cut-off distance of 1 nm, long-range electrostatic interactions were taken into account using the PME summation technique (Essman *et al*. 1995). The equilibrium state was determined by monitoring the size of the basic cell.

In a previous MD study (Boek *et al*. 2002), it was found that a bilayer membrane with carboxylate head groups develops a crystalline structure, where the erucyl tails are strongly ordered. The EHAC membrane on the other hand, was found to display liquid-crystalline phase behaviour. A snapshot of the EHAC membrane is shown in

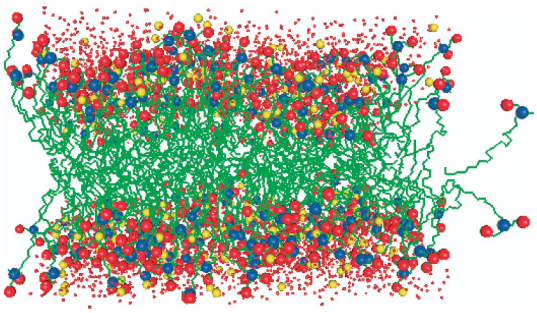

Figure 3. Snapshot of the EHAC bilayer membrane. Blue spheres, nitrogen; red spheres, head group oxygen; yellow spheres, chloride ions. The EHAC tails are represented as green sticks. The water hydrogen atoms are removed and the small red dots represent water oxygen atoms.

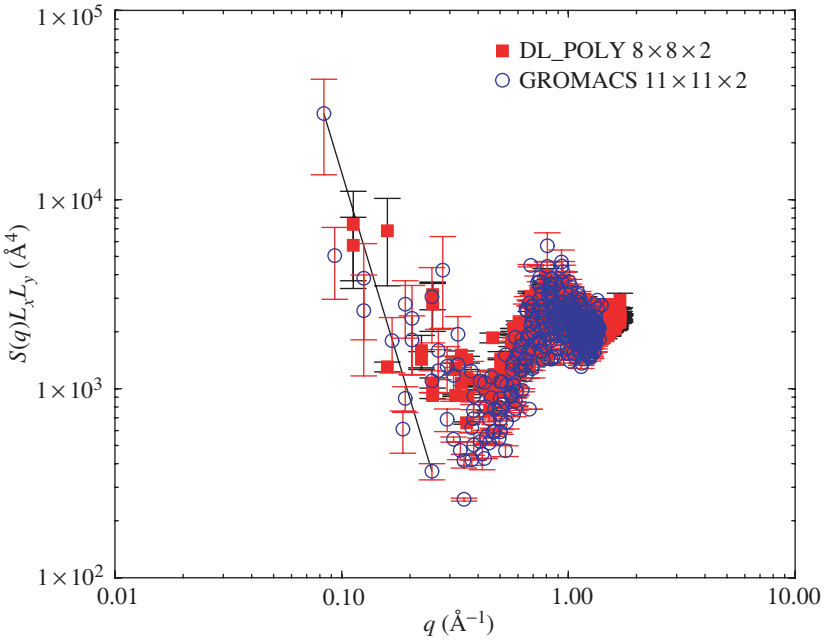

Figure 4. Structure factors for tensionless atomistic EHAC membranes: comparison of DL_POLY and GROMACS simulations. A black line following $\boldsymbol{q}^{-4}$ is added as a guide to the eye. See text for details.

figure 3. In the current study, we investigate the effect of this difference in head group chemistry on the bending rigidity of the bilayer membrane.

Because of the periodicity imposed on the bilayer by the periodic boundary conditions, the mid-plane of the bilayer membrane is expressed as a Fourier series

$$z(x,y) = \sum_{n_x}\sum_{n_y} c_{n_x n_y} \exp\left[2\pi \mathrm{i}\left(n_x \frac{x}{L_x} + n_y \frac{y}{L_y}\right)\right] + z_0, \tag{5.1}$$

where L_x and L_y are the dimensions of the membrane in the x- and y-directions, respectively. In order to determine the bending rigidity κ, we calculate the static structure factor $S(\boldsymbol{q})$. In the following, we will use both the structure factor and

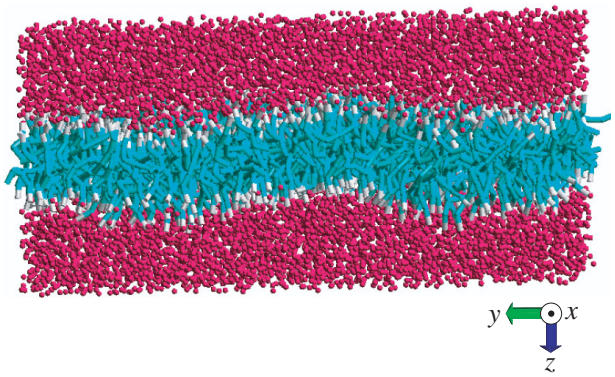

Figure 5. Snapshot of the coarse-grained bilayer membrane.
Red spheres, water; white cylinders, head groups; blue cylinders, surfactant tails.

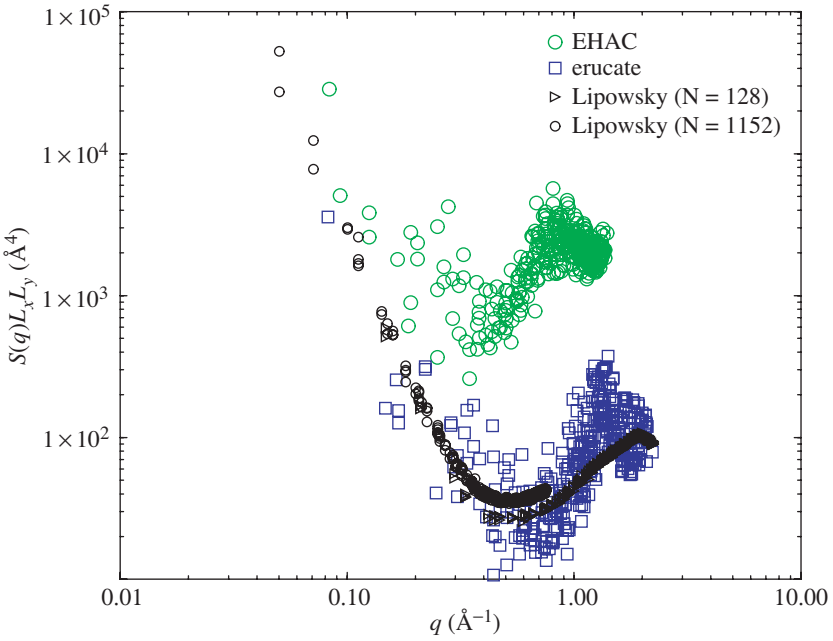

Figure 6. Structure factors for tensionless membranes: atomistic EHAC and erucate compared with the coarse-grained (Lipowsky) membranes (consisting of 128 and 1152 surfactants). See text for details.

fluctuation spectrum as interchangeable terms to indicate $S(\boldsymbol{q})$. For a tensionless membrane, the equipartition theorem yields

$$S(\boldsymbol{q}) = \langle c_{\boldsymbol{n}} c^*_{\boldsymbol{n}} \rangle = \frac{k_{\mathrm{B}}T}{\kappa L_x L_y} \boldsymbol{q}^{-4}, \tag{5.2}$$

with wavevector

$$\boldsymbol{q} = 2\pi \left(\frac{n_x}{L_x}, \frac{n_y}{L_y} \right). \tag{5.3}$$

Equation (5.1) can be formally inverted to express $c_{\boldsymbol{n}}$ as an integral over the perpendicular coordinate z. If we substitute the smooth plane by a series of Dirac delta peaks for all the atoms in the bilayer, we find

$$c_{\boldsymbol{n}} = \frac{1}{N}\sum_{i=1}^{N}(z_i - z_0)\exp\left[-2\pi\mathrm{i}\left(n_x\frac{x_i}{L_x} + n_y\frac{y_i}{L_y}\right)\right], \tag{5.4}$$

where $z_0 = N^{-1}\sum_i z_i$. Now we can verify whether the distributions observed in the simulations are in agreement with the prediction of equation (5.2). If this is the case, then we can extract a value for the bending rigidity κ. This method of calculating κ was successfully used by Goetz *et al.* (1999) and den Otter & Briels (2003) for CG membranes. Recently, atomistic membranes have been studied in this fashion by Lindahl & Edholm (2000) and Marrink & Mark (2001).

It is important to note that equation (5.2) is only valid when the membrane is in a state of zero surface tension. In order to find the tensionless state, we used a box scaling procedure using a modified Berendsen barostat (den Otter & Briels 2003), scaling L_x and L_y every time-step by a factor proportional to the pressure difference

$$\delta p = p_{zz} - \tfrac{1}{2}(p_{xx} + p_{yy}). \tag{5.5}$$

The perpendicular dimension L_z was scaled simultaneously, keeping the total volume of the simulation box constant. In this fashion, reasonable estimates of the box dimensions of the tensionless states were obtained. In a separate publication (Boek *et al.* 2004), we will report on a procedure to determine the tension free state and elastic modulus (see den Otter & Briels 2003) from a series of simulations whereby the x- and y-dimensions of the membrane were stretched or compressed in a series of small steps with respect to the box dimensions determined above, while keeping the total volume of the simulation box constant. From subsequent simulations carried out at constant volume, the pressure difference was found to be proportional with the area of the bilayer. The slope of this function then yields the area compressibility or elastic modulus of the membrane (Boek *et al.* 2004).

The membranes were run in the tensionless state for *ca.* 1 ns each, following equilibration runs of 0.5 ns. The inverse Fourier transform of equation (5.4) was calculated every 50 steps. The resulting structure factors, multiplied by L_xL_y, are shown in figure 4 as a function of the length of the wavevector $\boldsymbol{q}$. Several features can be distinguished in the fluctuation spectrum. A local maximum is observed at $q = 1.4$ Å^{-1}, corresponding to a wavelength $2\pi/q = 4.5$ Å. This value coincides with the location of the first peak in the radial distribution function for the EHAC head groups, corresponding to nearest-neighbour distances between surfactants in one leaflet of the bilayer membrane, as shown in fig. 12 of Boek *et al.* (2002). For smaller values of $\boldsymbol{q}$, the value of the structure factor increases, but it is not immediately clear whether the $\boldsymbol{q}^{-4}$ behaviour is recovered. This is due to the finite size of the membrane limiting the range of $S(\boldsymbol{q})$ to be observed for small $\boldsymbol{q}$. The fluctuation spectra for EHAC membranes using both the DL_POLY and Gromacs MD codes are presented in figure 4. It is interesting to observe that these spectra display very similar behaviour. This can be explained by realizing that the Coulomb part of the non-bonded interactions is the same for both models. Apparently, the different models for bonded and van der Waals interactions are unimportant in this respect, as is the effect of different membrane sizes used. This indicates that the fluctuation spectrum has general properties, largely independent of force field or system size used.

To clarify the behaviour for large wavelengths, we have also performed membrane simulations for a CG model surfactant. Using this model, introduced by Goetz *et al.* (1999), it is possible to study larger membranes at smaller computational cost than for the fully atomistic models. It is our objective to map the behaviour of the atomistic models on that of the CG model. Coarse-graining can be done with respect to many different observable quantities, both structural and dynamic; here we wish to coarse-grain with respect to the structure factor $S(\boldsymbol{q})$. We only discuss the main features of the CG surfactant model here; for more detail we refer to the original paper. The surfactant consists of one head and four tail particles, the latter representing three or four methyl groups each. The solvent particle, representing two water molecules, is identical to the head particle. Starting configurations were made by constructing two parallel layers of amphiphiles, heads pointing outwards. The rest of the simulation box was filled randomly with solvent particles. After minimization and equilibration, simulations were performed to achieve the tensionless state, using the algorithm described above. Two simulation boxes, containing 128 and 1152 surfactants each, were created in this fashion. A snapshot of the larger box is shown in figure 5.

We calculated the structure factors of these two CG membranes according to the method described above. The fluctuation spectra are shown in figure 6, together with the results for the atomistic membranes. It appears that, for large wavelengths, a linear regime is found with a slope of almost exactly minus four. From the intercepts, reliable values of the bending rigidities can now be extracted. It is possible to fine-tune the intermolecular potential parameters of the CG model to yield fluctuation spectra that coincide with the atomistic ones. This will be detailed in a forthcoming paper (Boek *et al.* 2004). From figure 6 it can already be observed qualitatively that the difference in head groups results in a dramatic difference in the fluctuation spectra of both atomistic membranes.

6. MD simulation of amphiphilic wormlike micelles

The simulations were carried out using the GROMACS (Lindahl *et al.* 2001; Berendsen *et al.* 1995) code under roughly the same conditions as described above for the membranes. The rods were constructed from 20 round slices placed along the z-direction with 16 surfactant molecules per slice. Every second slice was rotated to make the surface of the rod more uniform. However, the rod has a hole inside, due to the spatial structure of individual molecules. In order to avoid occupation of the hole by water and to provide a reasonable initial density of the hydrophobic core, the rods were shrunk in x- and y-dimensions. This was done in a series of steps followed by geometry optimization to relax stretched bonds. The end of the process was determined by visual inspection and monitoring of the potential energy. In order to maintain the shape of the rod, the number of steps of geometry optimization should be kept small to avoid displacement of molecules as a whole. The resulting structures were surrounded by SPC water and the number of counter ions required for charge neutrality. In this paper, we study two wormlike micellar systems. First, we consider EHAC-NaCl, containing EHAC surfactants and NaCl salt in a concentration of 3 wt % (which roughly corresponds to one salt molecule per 105 water molecules). Second, we consider EHAC-Sal-NaCl, which contains the same com-

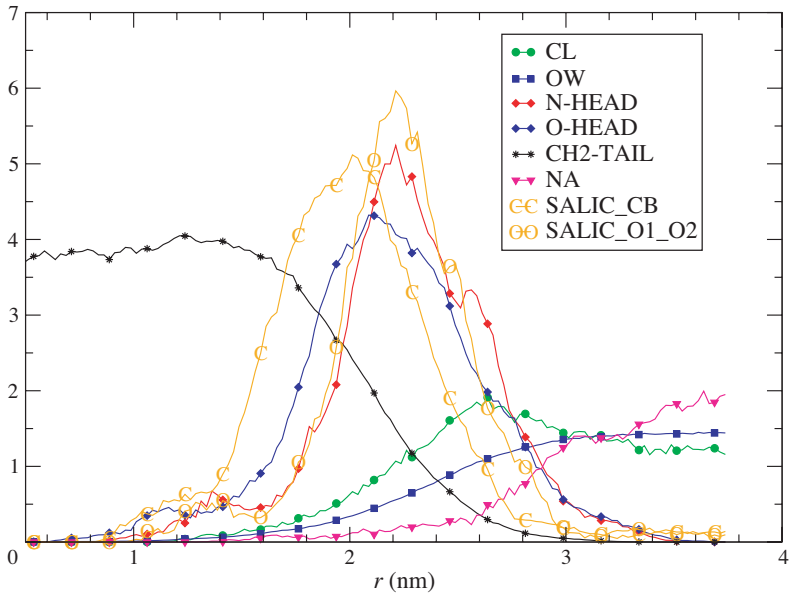

Figure 7. EHAC-Sal-NaCl detailed two-dimensional radial density distribution functions (the centre of the worm is taken as the reference point).

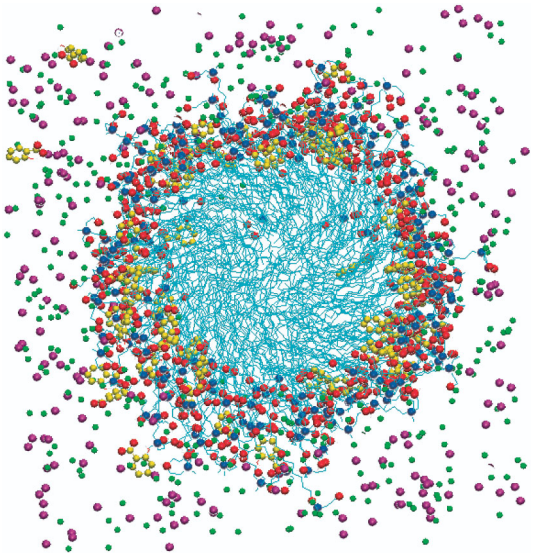

Figure 8. Snapshot (axial view) of the EHAC-Sal-NaCl system. Blue, nitrogen atoms; red, oxygen atoms; yellow, carbon atoms of the salicylate; green and magenta, chloride and sodium ions; cyan, carbon atoms of the surfactant's tail. Water is removed for clarity.

ponents as the EHAC-NaCl system, augmented with sodium salicylate molecules, taken as 25% of the number of the surfactant molecules, i.e. a 20:80 mixture. Both systems mentioned are considered as viscoelastic gels for hydraulic fracturing operations.

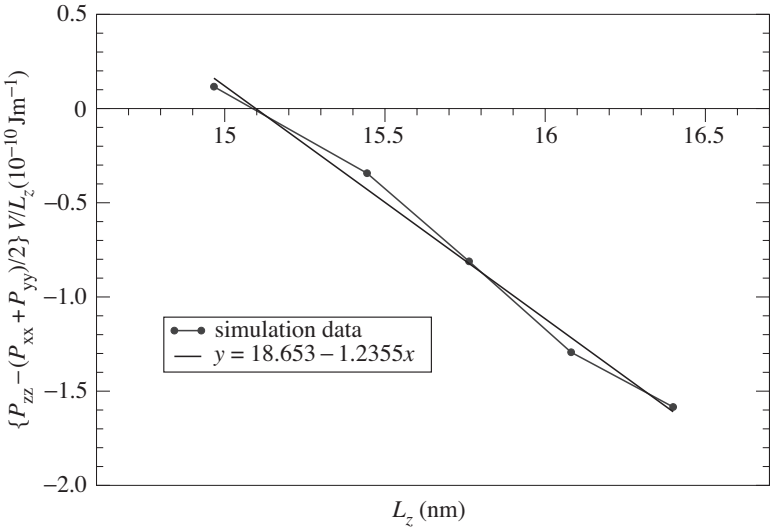

Figure 9. Pressure difference ΔP between directions parallel and perpendicular to the worm, as a function of the box length L_z.

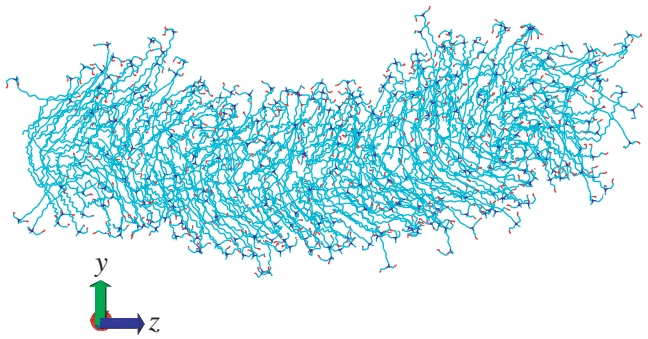

Figure 10. Side view of the EHAC-NaCl tensionless wormlike micelle.

(*a*) *Analysis of MD data*

Important properties of a wormlike micelle are the radius and the surface area per surfactant. These parameters are of value because they can be obtained from experiments. Clearly, the surface area depends on the value of the radius of the worm. In order to understand the structure of the rod and surrounding solution, one has to calculate the number of particles at a particular distance from the axis of the rod, i.e. the long axis running through the centre of mass. Hereafter we refer to this two-dimensional radial distribution function as the 'RDDF' (radial density distribution function). We are interested in the distribution of the head groups, CH_2 groups of the tail, salicylate residues, water molecules, chloride and sodium ions. We define the radius of the worm R_{rod} as the point at which the RDDFs of the CH_2-group and water's oxygen cross. The reason is that these RDDFs are smooth and the crossing-point is readily defined. A typical radius of the worm is 23–25 Å and the surface area per surfactant a is *ca.* 60–70 Å^2. The detailed RDDF of the system is given in figure 7.

The hydrophobic part (the benzene ring) of salicylate (labelled as SALIC_CB) penetrates into the hydrophobic core, while the oxygen atoms of the COO^- functional group closely interact with the nitrogen atom of the surfactant's head group. This observation is in good agreement with experimental results (Rehage & Hoffmann 1991). A snapshot of the molecular dynamics simulations clearly shows this effect (see figure 8).

(*b*) *Elastic modulus and persistence length*

The second part of the research is the evaluation of the mechanical properties of a rod-like micelle. These include the elastic modulus K_L and bending rigidity κ. It is important to determine the tensionless state of the rod to get the correct value for the bending rigidity, as described above. To achieve the tensionless state, we have run a series of constant volume (NVT) simulations for perturbed geometries of the basic cell. The technique is to squeeze (or expand) the cell in the z-dimension and calculate the pressure tensor. In order to keep the total volume of the cell constant, shrinking in z-direction must be accompanied by expanding in x- and y-directions, and vice versa. The simulation should be long enough to allow the system to equilibrate. To calculate the pressure tensor with acceptable accuracy, the production time should be long as well. For these reasons the evaluation of the elastic modulus is a very expensive task in terms of central-processing-unit time. For this reason, we performed simulations for the system EHAC with 3% NaCl only. The final configuration of the preceding NpT run, with a box z-dimension L_z of 15.92 nm, was taken as the initial structure for a series of NVT simulations. In order to find the tensionless state, the cell was expanded by a factor δ of 1.01 and 1.03 and shrunk by a factor of 0.99 and 0.97 in the z-dimension. This corresponds with values of L_z varying between 15.4 and 16.4 nm. Appropriate isotropic transformations in x and y dimensions were done to keep the volume of the basic cell the same over all the systems. The systems were allowed to relax for 1 ns. This was followed by a 1.5 ns production run. The final simulation has been run for the system shrunk by a factor $\delta = 0.94$ in the z-dimension, corresponding to $L_z = 15.0$ Å. All these points were fitted by a straight line (see figure 9). It was found that the tensionless state corresponds to $L_z = 15.1$ Å. We have not simulated the EHAC-NaCl system for that L_z because it is close enough to $L_z = 15.0$ (see figure 9). Hereafter, we refer to the system with $\delta = 0.94$ as the tensionless system. A snapshot of the tensionless worm is shown in figure 10.

We used the elastic-body approximation for the basic cell in the form given by den Otter & Briels (2003) to calculate the elastic modulus K_L:

$$-\Delta P \frac{V}{L_z} = \frac{K_L}{L_{z0}}(L_z - L_{z0}), \tag{6.1}$$

where L_{z0} is the box z-dimension in the tensionless state. Both K_L and L_{z0} can then be determined from a graph of $-\Delta PV/L_z$ as a function of L_z, as shown in figure 9. From a linear fit of all data points, we find $L_{z0} = 15.10$ nm and K_L to be of the order of 19×10^{-10} J m^{-1}. This is about four times greater than the reported value of 4.6×10^{-10} J m^{-1} for the CG model (den Otter *et al.* 2003). We will discuss this later.

The persistence length of the EHAC-NaCl system in the tensionless state can be evaluated by computing the structure factors $S_\alpha(q)$ which scale in accordance with

the equipartition theorem:

$$S_\alpha(n) = \langle c_{\alpha,n} c^*_{\alpha,n} \rangle = \frac{k_\mathrm{B}T}{L_z \kappa} q_n^{-4}, \quad q_n = \frac{2\pi}{L_z} n;\ \alpha = x, y, \tag{6.2}$$

where κ is the bending rigidity and $c_{\alpha,n}$ are the coefficients of the Fourier decomposition (den Otter *et al*. 2003).

We are currently in the process of calculating the fluctuation spectrum of the tensionless worm. The bending rigidity κ can then be found from a fit of the low-q modes to q^{-4}, see equation (6.2). Preliminary results indicate that, for the current size of our atomistic simulation box and a production time of 1.5 ns, the persistence length $l_\mathrm{p} = \kappa / k_\mathrm{B}T$ of the atomistic model is roughly four times larger than the CG model result of 130 Å (den Otter *et al*. 2003). (These results may still suffer from finite size effects and insufficient sampling of the low-q modes.) Note that the atomistic result is in qualitative agreement with experimentally observed values (Magid 1998) for the persistence length of 470 Å for the C_{16}TACl/NaCl system and *ca.* 1400 Å for C_{16}TASal/NaSal.

It seems that the CG model underestimates both the elastic and bending modulus. This indicates that the CG surfactant structures are too flexible. We consider the neglect of bending and dihedral potentials in the CG model as the origin of the discrepancy. In order to map the mechanical properties of the atomistic micelle on those of a CG micelle, the CG surfactant model will have to be adjusted. This will be reported in more detail in a separate publication.

We thank Geoff Maitland, Johan Padding, John Crawshaw, Henk Lekkerkerker, Arben Jusufi and Hartmut Loewen for their contributions to this work. W.K.d.O. and W.J.B. acknowledge financial support from the Stichting voor Fundamenteel Onderzoek der Materie (FOM), which is part of the Nederlandse Organisatie voor Wetenschappelijk Onderzoek (NWO).

References

Ben-Shaul, A. & Gelbart, W. M. 1994 In *Micelles, membranes, microemulsions and monolayers* (ed. W. M. Gelbart, A. Ben-Shaul & D. Roux), ch. 1. Springer.

Berendsen, H. J. C., Postma, J. P. M., van Gunsteren, W. F. & Hermans, J. 1981 In *Intermolecular forces* (ed. B. Pullman). Dordrecht: Reidel.

Berendsen, H. J. C., van der Spoel, D. & van Drunen, R. 1995 *Computat. Phys. Commun.* **91**, 43–56.

Boek, E. S., Jusufi, A., Loewen, H. & Maitland, G. C. 2002 *J. Phys. Condens. Matter* **14**, 9413–9430.

Boek, E. S., Chin, J. & Coveney, P. V. 2003 *Int. J. Mod. Phys.* B **17**, 99–102.

Boek, E. S., den Otter, W. K. & Briels, W. J. 2004 Mechanical properties of atomistic surfactant bilayer membranes from molecular dynamics simulations by mapping on a coarse grained amphiphile model. (Submitted.)

Cates, M. E. 1988 *J. Phys. France* **49**, 1593.

den Otter, W. K. & Briels, W. J. 2003 *J. Chem. Phys.* **118**, 4712.

den Otter, W. K., Shkulipa, S. A. & Briels, W. J. 2003 *J. Chem. Phys.* **119**, 2363.

Essman, U., Perera, L., Berkowitz, M. L., Darden, T., Lee, H. & Pedersen, L. G. 1995 *J. Chem. Phys.* **103**, 8577–8592.

Goetz, R., Gompper, G. & Lipowsky, R. 1999 *Phys. Rev. Lett.* **82**, 221.

Lindahl, E. & Edholm, O. 2000 *J. Chem. Phys.* **113**, 3882.

Lindahl, E., Hess, B. & van der Spoel, D. 2001 *J. Mol. Model.* **7**, 306–317.
Magid, L. J. 1998 *J. Phys. Chem.* B **102**, 4064–4074.
Marrink, S. J. & Mark, A. E. 2001 *J. Phys. Chem.* B **105**, 6122.
Miyamoto, S. & Kollman, P. A. 1992 *J. Comput. Chem.* **13**, 952–962.
Raghavan, S. R. & Kaler, E. W. 2001 *Langmuir* **17**, 300.
Rehage, H. & Hoffmann, H. 1991 *Molec. Phys.* **74**, 933–973.
Smith, W. & Forester, T. 1996 *J. Mol. Graphics* **14**, 136.